

Upper Mantle Seismic Structure Beneath Southern Africa: Constraints on the Buoyancy Supporting the African Superswell

MARTIN B. C. BRANDT,^{1,2} STEPHEN P. GRAND,³ ANDREW A. NYBLADE,⁴ and PAUL H. G. M. DIRKS^{2,5}

Abstract—We present new one-dimensional SH-wave velocity models of the upper mantle beneath the Kalahari craton in southern Africa obtained from waveform inversion of regional seismograms from an $M_w = 5.9$ earthquake located near Lake Tanganyika recorded on broadband seismic stations deployed during the 1997–1999 Southern African Seismic Experiment. The velocity in the lithosphere beneath the Kalahari craton is similar to that of other shields, and there is little evidence for a significant low velocity zone beneath the lithosphere. The lower part of the lithosphere, from 110 to 220 km depth, is slightly slower than beneath other shields, possibly due to higher temperatures or a decrease in Mg number (Mg#). If the slower velocities are caused by a thermal anomaly, then slightly less than half of the unusually high elevation of the Kalahari craton can be explained by shallow buoyancy from a hot lithosphere. However, a decrease in the Mg# of the lower lithosphere would increase the density and counteract the buoyancy effect of the higher temperatures. We obtain a thickness of 250 ± 30 km for the mantle transition zone, which is similar to the global average, but the velocity gradient between the 410 and 660 km discontinuities is less steep than in global models, such as PREM and IASP91. We also obtain velocity jumps of between 0.16 ± 0.1 and 0.21 ± 0.1 km/s across the 410 km discontinuity. Our results suggest that there may be a thermal or chemical anomaly in the mantle transition zone, or alternatively that the shear wave velocity structure of the transition zone in global reference models needs to be refined. Overall, our seismic models provide little support for an upper mantle source of buoyancy for the unusually high elevation of the Kalahari craton, and hence the southern African portion of the African Superswell.

Key words: Southern Africa, African superswell, upper mantle, shear wave, velocity model, inversion.

1. Introduction

The “African Superswell” is one of the largest topographic anomalies on Earth that is not accounted for by a variation in crustal thickness or normal plate cooling. There is about 500 m of positive residual elevation covering eastern Africa, southern Africa (including the Kalahari craton) and an area of the southeastern Atlantic Ocean basin southwest of the African continent (NYBLADE and ROBINSON, 1994; NYBLADE and LANGSTON, 1998). One hypothesis to explain the uplift of southern Africa is that there is a large-scale, positively buoyant structure within the mid-lower mantle (LITHGOW-BERTELLONI and SILVER, 1998; GURNIS *et al.*, 2000) which causes viscous flow to uplift the surface. This is based on global seismic tomography results which have consistently shown the existence of a large-scale, low-shear-velocity anomaly beneath the African plate, extending from the core-mantle boundary to about 1,500 km depth (RITSEMA *et al.*, 1999; MASTERS *et al.*, 2000; MEGNIN and ROMANOWICZ, 2000; GU *et al.*, 2001; GRAND, 2002). The large-scale upward extension rises from its base under southern Africa into the midmantle, tilting towards eastern Africa (SIMMONS *et al.*, 2007). This megastructure was first mapped with global P-waves (e.g., DZIEWONSKI, 1984; HAGER *et al.*, 1985), but the shear wave velocity is up to three percent slower than that of the average mantle (e.g., RITSEMA *et al.*, 1998; RITSEMA *et al.*, 1999) in comparison with the closer-to-average compressional velocity. This velocity anomaly became known as the “African

¹ Seismology Unit, Council for Geoscience, Private Bag X112, Pretoria 0001, South Africa. E-mail: martinb@geoscience.org.za

² School of Geosciences, University of the Witwatersrand, Johannesburg, South Africa. E-mail: paul.dirks@wits.ac.za

³ Jackson School of Geosciences, University of Texas at Austin, Austin, TX, USA. E-mail: steveg@jsg.utexas.edu

⁴ Department of Geosciences, Pennsylvania State University, University Park, Pennsylvania, USA. E-mail: andy@geosc.psu.edu

⁵ School of Earth and Environmental Sciences, James Cook University, Townsville, Australia.

Superplume” (e.g., GURNIS *et al.*, 2000) and SKS phase waveform modeling mapped it with sharp sides (e.g., NI *et al.*, 2002; NI *et al.*, 2005). However, the global tomography images of the Superplume do not show a connection from the lower mantle to the lithospheric mantle, except perhaps under the East African Rift.

Despite the lack of a connection between the African Superplume and the lithospheric mantle, authors such as VINNIK *et al.* (1996) have suggested upper mantle buoyant support for the Superswell; these authors found anomalously low S-wave velocity from 370 to 470 km beneath southern Africa. QIU *et al.* (1996) and PRIESTLEY (1999) used surface waves to image upper mantle shear velocities and found a relatively thin lid with a strong S-wave low-velocity zone (LVZ) beneath southern Africa. BLOCH *et al.* (1969) and later LI and BURKE (2006) and PRIESTLY *et al.* (2006) also found evidence for a proposed LVZ in the uppermost mantle under southern Africa. By contrast, FREYBOURGER *et al.* (2001) and LARSON *et al.* (2006) found little evidence for a proposed LVZ. WANG *et al.* (2008) modeled the triplicated body-waves that propagated beneath southern Africa and found a very prominent LVZ zone, implying an anomalously hot upper mantle beneath southern Africa. Although teleseismic tomography results from southern Africa show little evidence for unusually slow upper mantle seismic velocities, which may represent a source of upper mantle buoyancy (FOUCH *et al.*, 2004), resolution in the deeper upper mantle is limited. Thus whether or not southern Africa is indeed underlain by an anomalously, seismically slow buoyant mantle is still not clear.

The deeper upper mantle has been investigated using receiver functions (GAO *et al.*, 2002; NIU *et al.*, 2004), but little evidence has been found for an unusual transition zone beneath southern Africa that would indicate a thermal anomaly within the deep upper mantle (e.g., BINA and HELFFRICH, 1994). BLUM and SHEN (2004) actually found a shallowing of the 410 km discontinuity and a deepening of the 660 km discontinuity, and thus a mantle transition zone 20 km thicker than the global average, which would imply a colder transition zone.

NYBLADE and SLEEP (2003) proposed an upper mantle source of buoyant support for the Superswell from plume material that may have ponded beneath the cratonic lithosphere from the Mesozoic onward when several large magmatic events occurred (e.g. TANKARD *et al.*, 1982) to produce the present-day elevation. Their model predicts ~ 25 km of lithospheric thinning beneath the craton and a global average LVZ under the lithosphere because Mesozoic plume material would not be hotter than today’s mantle adiabat. A small decrease in seismic wave speeds throughout the lithosphere is expected because excess heat from the plumes would diffuse slowly through the lithosphere over many tens of millions of years. For example, the temperature change at 100 km depth of ~ 90 K in Nyblade and Sleep’s model implies a P-wave velocity reduction of 0.05 km/s using a temperature P-wave velocity derivative of -5×10^{-4} km/s/K.

The objective of our study is to investigate the shear wave velocity structure of the upper mantle under southern Africa using regional waves. The S-waves that turn in the upper mantle are the most sensitive to shear velocity as a function of depth. The 410 and 660 km discontinuities, which form the boundary of the transition zone, produce triplications for these waves and thus complicated waveforms. Upper mantle turning waves have yielded detailed models of the transition zone and lithosphere before, but these seismic models are often constructed by trial and error, making the resolution provided difficult to assess.

Another common problem with past studies using turning waves is that sometimes a 1-D model is extracted from data from various earthquakes that actually sample fully 3-D structures. It has been difficult to assess the effect of these 3-D variations on the models. In our investigation we use a waveform inversion technique on data sets of SH upper mantle triplicated phases generated from one well-recorded earthquake to derive two regional 1-D shear wave velocity models beneath southern Africa (Fig. 1). The waveform inversion technique produces an optimal data fit with some a priori constraints. The earthquake is recorded by a dense array of seismic stations in southern Africa that allow single profiles to be

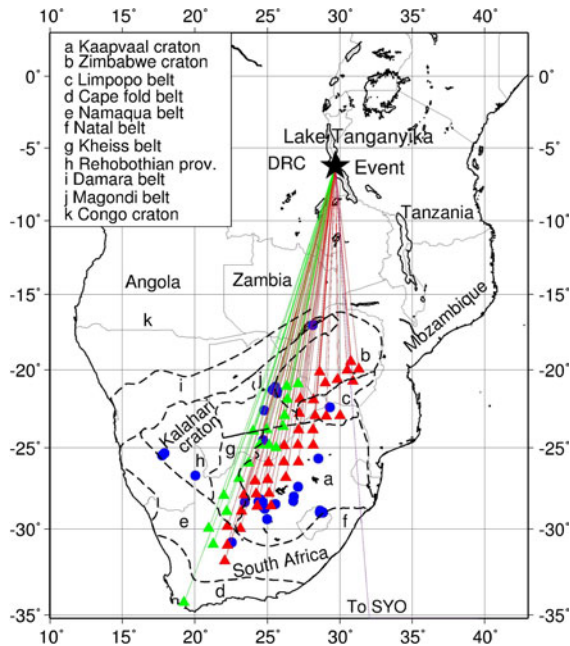


Figure 1

Location map of the seismic stations and earthquake used in this study. A black star indicates the earthquake position. Red triangles show the stations used to derive the eastern model and green triangles the central model. The red and green lines represent the areas where the waves turn and thus sample the lithosphere, shallow mantle above 410 km depth and the transition zone (see profile in Fig. 2b). The purple line represents the wave path recorded by station SYO used to determine the source-time function. Major tectonic provinces are separated with dashed lines and are indicated with minor letters a–k. Blue dots represent the positions of kimberlites from which xenoliths were analyzed (taken from GRIFFEN *et al.*, 2003)

sampled, thus minimizing problems with the 3-D structure.

In previous seismic studies of southern Africa using regional phases, P-wave speed models were derived for the upper mantle using a Herglotz-Wiechert method combined with ray tracing, and followed by stacking and synthetic seismograms (SIMON *et al.*, 2002; WRIGHT *et al.*, 2002). This approach was later extended to include S-waves by SIMON *et al.* (2003), who found a seismic lid about 210 km thick. ZHAO *et al.* (1999) investigated the P- and S-wave velocity structure using a Herglotz-Wiechert method with data recorded in Tanzania. Limited S-wave travel-time data suggest fast S-wave velocities above ~ 150 km depth, but not buoyant support for the Superswell in the upper mantle. WANG *et al.* (2008) recently studied the SH- and P-wave

upper mantle velocity structure beneath southern Africa. They used a limited number of models to do trial-and-error modeling of the waveforms of triplicated waves. They also used a different frequency band than we use, namely 1–50 s and not 5–100 s, and a different source origin time. Their models have a high-velocity lid that is 150 km thick, with a strong LVZ beneath. They conclude that the LVZ could have a low density and thus provide some of the buoyancy supporting the African Superswell. Here we extend the study by WANG *et al.* (2008), using a different approach, to match the waveforms and obtain a very different result. We feel our model better fits later arrivals that are most sensitive to the velocities from 200 to 400 km depth where WANG *et al.* (2008) derived the strong LVZ.

2. Data and Observations

The IRIS PASSCAL Kaapvaal southern African seismic experiment involved 55 broadband REFTEK/STS2 instruments, deployed at 81 sites, and was conducted between April 1997 and July 1999 (CARLSON *et al.*, 1996). The seismometers were arranged along a roughly NE–SW axis in southern Africa in the countries of South Africa, Botswana and Zimbabwe. The continuously recorded data from the portable experiment were supplemented by data from three global digital stations in the region of the array (e.g., NGUURI *et al.*, 2001). We used IRIS Kaapvaal array seismic waveform data produced by a shallow $M_w = 5.9$ earthquake located at Lake Tanganyika on 21 September 1997 (Table 1). The IRIS Kaapvaal array spanned a distance of 12.1° – 28.7° from this event. The stations lie approximately along a large great circle from the event (Fig. 1). Great circles connect the epicenter to the seismograph stations in the eastern (red) and central (green) profiles. This makes these data ideal for investigating the detailed structure of the uppermost mantle and the mantle transition zone beneath eastern and central southern Africa. In addition, the compositional structure and thermal state of the lithospheric mantle beneath the Kalahari craton and surrounding belts have been mapped in space and time with garnet xenocrysts from kimberlites which intruded over the period

Table 1
Event parameters of the Lake Tanganyika earthquake of 1997/09/21

Time	Latitude	Longitude	Depth	Magnitude	Strike	Dip	Rake	Agency
18:13:22.78	−7.36	30.37	10	5.9 Mw	320	24	−124	NEIC
18:13:32.5	−7.29	30.27	30	5.9 Mw	315	36	−133	HRV
18:13:23.0	−7.343	30.287	10	5.8 Ms				MOS
18:13:23.6	−6.88	30.18	8	5.9 Ms				BJI
18:13:26.87	−7.387	30.330	24					EHB
18:13:28.3	−7.4068	30.3414	37.8	4.7 mb				EIDC

NEIC National Earthquake Information Centre, *HRV* Harvard Centroid Moment Tensor, *MOS* Moscow, Russian Academy of Sciences, *BJI* Beijing, China Earthquake Administration, *EHB* Engdahl, van der Hilst and Buland, University of Colorado, *EIDC* Experimental International Data Centre, Arlington, US

520–80 Ma (GRIFFIN *et al.*, 2003; WILSON *et al.*, 2007).

The focal mechanism parameters for the earthquake were taken from the Harvard Centroid Moment Tensor catalogue (HRV). The depth of the earthquake, as reported by all the hypocenter agencies, varies between 8 and 37.8 km. We determined a depth of 27 ± 2 km for the event by fitting the sS phase waveform at station SYO at Syowa Base on Antarctica at an epicentral distance of 61.9° (Fig. 2a). The velocity seismograms in Fig. 2a were bandpass filtered from 0.01 to 0.1 Hz. This is the nearest teleseismic station with the same azimuth as the regional data we modeled. The source time function was derived by forward modeling the seismogram recorded at this station. We determined an origin time of 18:13:27.5 from the average time of all the reporting agencies, corrected for our source depth of 27 km. The observed seismograms for eastern and central southern Africa were initially shifted in time to account for topography and crustal thickness variations along the array. This was done so that the arrival times of the data would correspond to those expected for a 35 km thick crust with zero topography. To make the time corrections we used the crustal models of NGUURI *et al.* (2001) and STANKIEWICZ *et al.* (2002). Their models show that the undisturbed Archean craton crust is typically thin (35–40 km), unlayered and has a strong velocity contrast across a sharp Moho discontinuity. In addition, modified receiver functions obtained from high-quality data from a dense seismic array near Kimberley showed a crustal thickness of 35.4 km and a flat, sharp Moho transition zone of less than 0.5 km (NIU and JAMES,

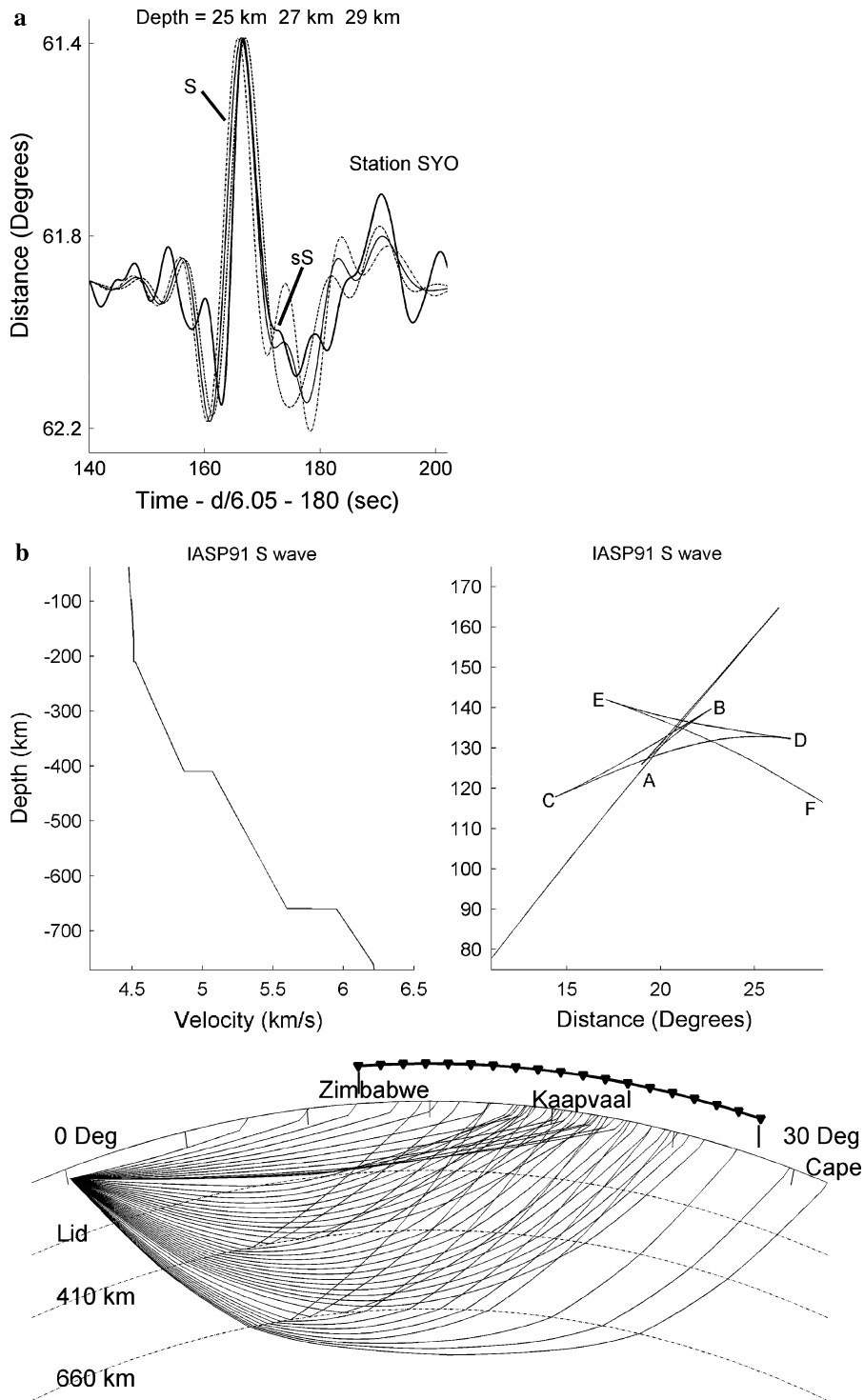
2002). We also added 1 s to the arrival times of the most distant stations, which are situated off the Kaapvaal craton on the Namaqua and Cape Fold belts (Fig. 1). This addition was based on the results of seismic tomography by FOUCH *et al.* (2004) who found a 1.2% decrease in shear wave velocity in the shallow mantle beneath these regions.

Figure 2b shows the S-wave IASP91 model, as well as the ray paths and travel-time curve computed using IASP91 for upper mantle distances. Because of discontinuities near 410 and 660 km depth, multiple arrivals are produced at certain distances. The time separation of the different branches (A–F in Fig. 2b) with distance is sensitive to the velocity gradient between the discontinuities and to the velocity increases across the discontinuities. The Zimbabwe and Kaapvaal cratons, Cape Fold Belt and seismic

Figure 2

a Tangential component seismogram (SH-wave) recorded by station SYO at Syowa Base on Antarctica at a distance of 61.9° . The *heavy line* shows the data. Synthetic seismograms generated using the IASP91 seismic model are shown for a depth of 25 km (*dashed line*), the best fit depth of 27 km (*thin line*) and 29 km (*dash-dot line*). The direct S and up-going sS arrivals are labeled. The time scale is shown with a reduction velocity of 6.05 km/s – 180 s, where d is the epicentral distance in degrees. **b** The IASP91 shear velocity model (*top left*). The travel-time curve for the IASP91 shear velocity model for a source at 27 km depth is shown at the *top right*. Branch AB represents direct arrivals that turn above the 410 km discontinuity; at small distances these arrivals turn within the lithosphere. Branch CD represents arrivals turning within the transition zone from 410 to 660 km depth, and branch EF corresponds to waves that have turned below the 660 km discontinuity. The ray paths for the IASP91 model are shown at the bottom. The Zimbabwe and Kaapvaal cratons, Cape fold belt and seismic stations are labeled on the profile

Upper Mantle Seismic Structure



stations are labeled above the profile to determine where a specific turning wave samples the region.

A preliminary examination of the Kaapvaal data showed a clear difference in waveforms for the

central stations relative to the eastern stations. Onsets for the first phase at close distances differ by 2 s (Fig. 3a). We, therefore, divided the data into two profiles sampling eastern and central southern Africa.

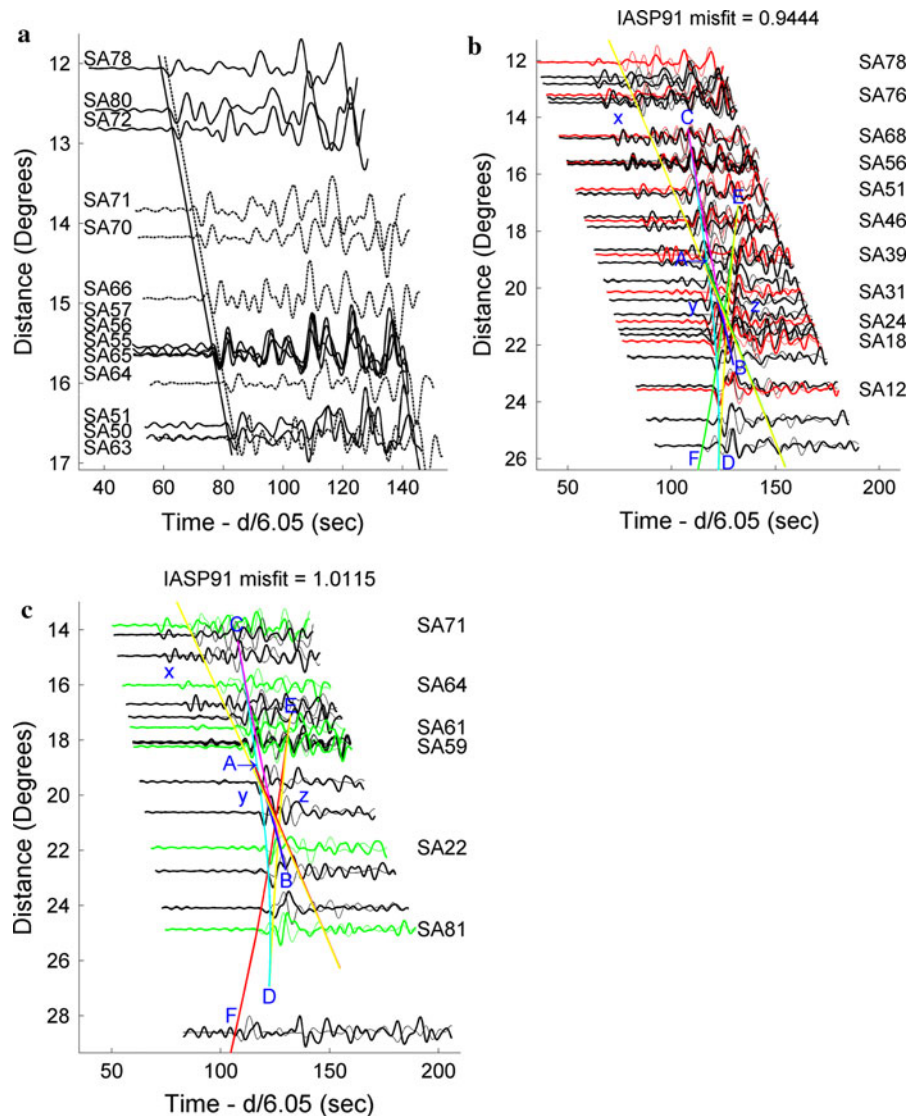


Figure 3

a Tangential component seismograms (SH waves) recorded by the eastern (*solid lines*) and central (*dashed lines*) stations between the distances of 12° and 17°. Onsets for the first phase are connected by lines. Station names are listed on the *left*. The time scale is shown with a reduction velocity of 6.05 km/s, where d is the epicentral distance in degrees. **b** Tangential component seismograms (SH-waves) recorded by the eastern stations. The *heavy lines* show the data and the *thin lines* show synthetic seismograms generated using the IASP91 seismic model. The station names of every third trace (in *red*) are listed on the right. The travel-time curves predicted by IASP91 are overlaid on the data in multiple colors. Symbols A, B, C, D, E and F refer to the travel-time curve for upper mantle distances (see curves in Fig. 2b). Symbols x , y and z refer to the phase arrivals described in the text. The model misfit calculated with Eq. 2 is shown at the *top*. The time scale is shown with a reduction velocity of 6.05 km/s, where d is the epicentral distance in degrees. **c** Tangential component seismograms (SH-waves) recorded by the central stations. The *heavy lines* show the data and the *thin lines* show synthetic seismograms generated using the IASP91 seismic model. The station names of every third trace (in *green*) are listed on the right. The travel-time curves predicted by IASP91 are overlaid on the data in multiple colors. Symbols A, B, C, D, E and F refer to the travel-time curve for upper mantle distances (see curves in Fig. 2b). Symbols x , y and z refer to the phase arrivals described in the text. The model misfit calculated with Eq. 2 is shown at the *top*. The time scale is shown with a reduction velocity of 6.05 km/s, where d is the epicentral distance in degrees

Figure 3b and c show the IRIS Kaapvaal and global station SH-wave recordings (tangential component) for eastern and central southern Africa respectively,

and the corresponding synthetic seismograms computed using the IASP91 (KENNETT and ENGD AHL, 1991) shear velocity model. The synthetics were

computed using the reflectivity method (FUCHS and MÜLLER, 1971). The velocity seismograms in Fig. 3a, b and c were bandpass filtered from 0.01 to 0.2 Hz. At the distances shown in Fig. 3b and c, direct S-waves turn within the upper mantle, with turning depths ranging from the seismic lid to the transition zone depending on distance. Figure 3b and c plot the IASP91 travel-time curves on the data. An initial, fast arrival labeled with an x in Fig. 3b and c turns within the lid and can be clearly seen in the data. Multiple arrivals, labeled y and z , can be seen to join with distance. The IASP91 model predicts a single, direct arrival, which will sample the lithosphere at a distance of less than $\sim 14^\circ$, and two arrivals (which will eventually join together) sampling the lithosphere at greater distances. Comparison of the data and the IASP91 predictions shows that the fast arrival, labeled x in the data, is not predicted by the IASP91 model. This implies that a much faster lithosphere must exist beneath the northern part of the Zimbabwe craton, as well as beneath the Magondi and Damara belts, than accounted for in the IASP91 model. In both the data and the synthetics multiple arrivals are observed, but the relative timing of the arrivals does not match up. This indicates that the mantle above and within the transition zone beneath the Zimbabwe and Kaapvaal cratons and the Limpopo belt must be different from those of the IASPI91 model. Note that the rays shift from east to west under southern Africa for the eastern profile in Fig. 1 as the turning waves progressively sample deeper mantle structure.

3. Inversion Procedure

To invert the waveform data shown in Fig. 3b and c we use an iterative technique that utilizes a conjugate gradient algorithm. This algorithm was originally applied to seismology by MORA (1988), further developed by MATZEL and GRAND (2004), and applied by GAO *et al.* (2006) to a linear profile of upper mantle seismic waveforms in North America. We briefly review the approach here. The forward problem is

$$\underline{d}_n = \underline{d}(\underline{m}_n) \quad (1)$$

where \underline{d}_n are synthetic seismograms computed for model \underline{m}_n at iteration n , and \underline{d} is a nonlinear operator

that maps model space into the data space. Our objective is to find a model \underline{m}_n that best fits the seismic observations \underline{d}_{obs} by minimizing the difference between the synthetic and observed waveforms $\Delta \underline{d} = \underline{d}_n - \underline{d}_{obs}$. This difference can be quantified by a cross-correlation, where 0 = perfect fit and 1 = total misfit. The conjugate gradient technique iteratively minimizes the misfit function $S(\underline{d}, \underline{m})$ with

$$S(\underline{d}, \underline{m}) = 1/2[\Delta \underline{d}^T C_d^{-1} \Delta \underline{d} + \Delta \underline{m}^T C_m^{-1} \Delta \underline{m}] \quad (2)$$

where C_d and C_m are the covariance matrices for the data and model space respectively, and $\Delta \underline{m} = \underline{m}_n - \underline{m}_0$ is the difference between the starting model and the inverted model. An immediate solution is obtained by using the gradient vector to calculate the conjugate vector and the step length which subsequently determines the model update. For the scalar misfit, function 0 = perfect fit and 1 = total misfit.

The gradient vector is defined as the direction of steepest descent in model space. The conjugate direction is found by using the Polak-Ribière method and after the step length has been calculated, an optimization with a line search yields the model update (MATZEL, 2002). We use the reflectivity method (FUCHS and MÜLLER, 1971) to generate the synthetics and the differential seismograms. The conjugate gradient algorithm converges rapidly for upper mantle waveform problems and it iteratively minimizes the difference between data and synthetics in a least-squares sense to find the best-fitting model.

A difficulty with linearized waveform inversion is that if the starting model predicts synthetics that are more than half a cycle different from the data, the inversion can converge to a wrong model and will then predict synthetics one cycle off from the data. Since the conjugate gradient method will find the closest local minima, inversion results depend on the starting model. To solve this problem we derive a top-down solution for our Earth model in which the data most sensitive to the crust and lithospheric mantle are fit first and then the deeper mantle structure is solved for. We also begin with longer period filters and then progressively model broader-band data. This results in a starting model for the deeper mantle structure that has better alignment of arrivals, which reduces the cycle-skipping problem. We accomplish this by selecting decreasing time

windows for successive inversions, i.e., an intermediate result is the input for the next run. A large time window includes fundamental-mode surface waves which have the largest amplitudes and are most sensitive to lithospheric mantle structure. For this reason, in successive iterations we did not include the fundamental-mode surface waves so that instead the inversion focused on fitting deeper turning waves.

We selected as our starting model for the crust a multiple-layer structure based on the CRUST5.1 model (MOONEY *et al.*, 1998) and for the lithospheric mantle the seismic structure of the east European platform (MATZEL and GRAND, 2004), padded with the global PREM model (DZIEWONSKI and ANDERSON, 1981) below 220 km depth. Values for attenuation and density are based on the PREM model (DZIEWONSKI and ANDERSON, 1981). Preliminary forward modeling indicated a reasonable fit of synthetics to data for this starting model (synthetic phase arrivals occur more or less at the same time, but waveform amplitudes and/or patterns differ due to differences in joining/diverging phase arrivals), as opposed to the

poor fit yielded by the global reference models (synthetics are out of phase with the data).

Four example seismograms and their best-fit synthetics are shown in Fig. 4a. The higher-frequency body-wave arrivals are not clear for these data at this intermediate stage of our inversion procedure. Numbers refer to cross-correlations to estimate fits. Note that 0 means a perfect fit. The trace from station SA55 with a cross-correlation value of 0.1905 is one of five isolated poor fits, two of which are from the furthest stations off the Kaapvaal craton. The higher frequencies, and hence very shallow surface waves, of these poor fits could be affected by the attenuation, Q , which we kept constant throughout the inversions. Figure 4b is a close-up of the model resulting from inversion of the eastern data filtered with the long-period bandpass. This was then used as the starting model for the body-wave inversion for eastern southern Africa. Other starting models are also discussed below.

Next we solved for the deeper upper mantle structure by progressively employing smaller time

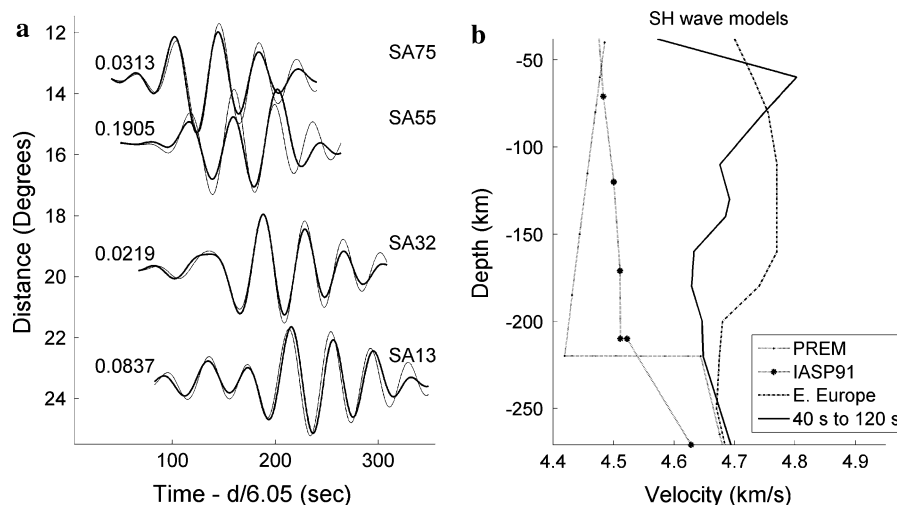


Figure 4

a Four examples of eastern tangential component synthetics (*thin lines*) and data (*heavy lines*) after inversion for the crust and lithospheric mantle. The long time window includes fundamental-mode surface waves. Data are filtered from 40 to 120 s. The station names are listed on the *right*. The numbers refer to cross-correlations used to estimate the fits between synthetics and data described in the text. **b** Comparison of the inverted model for 40–120 s Love waves (*solid line*) of the uppermost mantle with the IASP91 model (*dotted line with stars*) and the PREM model (*dotted line with small circles*) for eastern southern Africa. The *dash-dot line* is the starting model taken from the seismic structure of the east European platform derived from the same type of data, i.e., 10–20 s period regional SH waves (MATZEL and GRAND, 2004). The derived Love wave model (*solid line*) is used as the starting model for the eastern profile body waveform inversion

windows focused on the mantle body waves filtered between 5 and 100 s. Since stacked receiver functions have mapped the 410 and 660 km discontinuities at their average depths (GAO *et al.*, 2002) or within 20 km of the global average (BLUM and SHEN, 2004), we put these discontinuities at 410 km and 660 km depth, respectively, in the starting model. We deem the phase transition thickness to be 20 km across the 410 km discontinuity (i.e. 400–420 km) and the 660 km discontinuity (i.e. 650–670 km) (MELBOURNE and HELMBERGER, 1998). Synthetics are calculated with 10 km-thick layers, but the model parameters in the inversion are averaged velocities over 20–30 km. Time windows are selected to solve jointly for the phase arrivals for the lid and mantle transition zone (Figs. 3b, c, 5a, b). A problem with this approach is that the phases with larger amplitudes from the deeper upper mantle dominate the inversion results. For this reason we increased the sensitivity of the inversion to the initial, small phases in the time window by using the square root of the seismic traces.

We first derived the velocity model for eastern southern Africa using the procedure described above. Then we inverted for the velocity structure of central southern Africa, using the eastern model

as the starting model. The final synthetic to data best-fit waveforms and predicted travel-time curves are shown in Fig. 5a and b for eastern and central southern Africa. The corresponding final models are shown in Fig. 6 compared with the PREM and IASP91 models. The shallow eastern and central southern African velocity models are very similar, except above 110 km depth where the eastern profile is faster by a maximum of 0.09 km/s. Below 220 km the models differ by no more than 0.03 km/s, except around the 410 km discontinuity where they differ by up to 0.08 km/s. Both models have high velocities in the shallow mantle relative to PREM and IASP91 with very slight LVZs beneath. The velocity gradient above the 410 km discontinuity is similar to that of the PREM model: there are velocity jumps of 0.16 km/s (3.1% eastern) and 0.21 km/s (4.3% central) versus the 3.4% of the PREM model. Overall, the mantle transition zone is slower than that of the global models, with a correspondingly less-steep velocity gradient between the discontinuities. In particular, our models are slower than the PREM and IASP91 models from near 500 to 650 km depth, and the central model is even slower than the eastern model by up to 0.09 km/s.

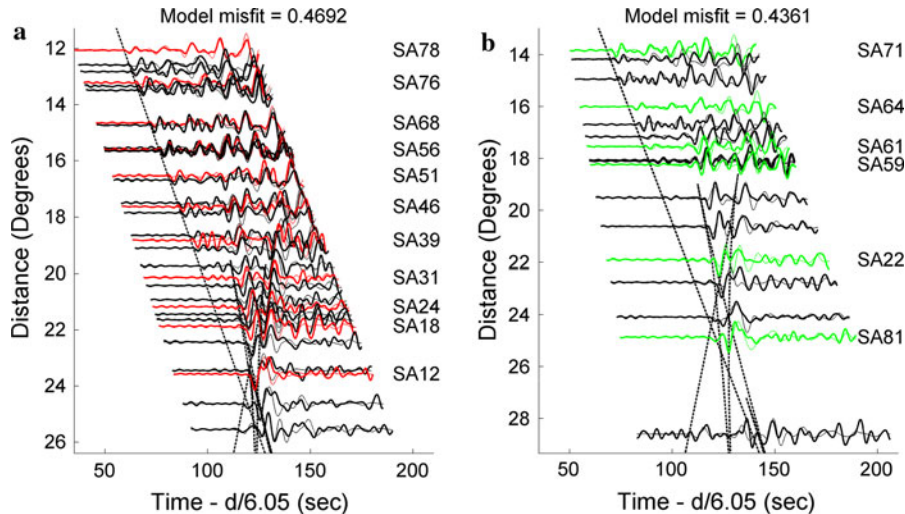


Figure 5

a. Comparison of data and synthetics for the eastern stations. The *thicker lines* show the data and the *thinner lines* the synthetics. The station names of every third trace (in red) are listed on the right. Predicted travel-time curves are overlaid on the traces. The model misfit calculated with Eq. 2 is shown at the top. **b** Comparison of data and synthetics for the central stations. The *heavy lines* show the data and the *thin lines* the synthetics. The station names of every third trace (in green) are listed on the right. Predicted travel-time curves are overlaid on the traces. The model misfit calculated with Eq. 2 is shown at the top.

The model misfit calculated with Eq. 2 is shown at the top

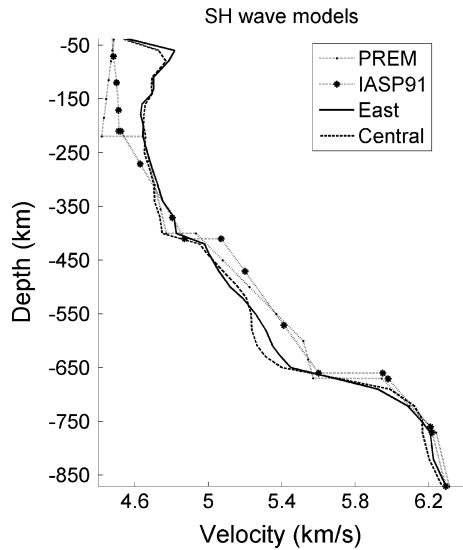


Figure 6

Comparison of the eastern southern Africa SH velocity model (*heavy line*) with the central southern Africa model (*dashed line*). The *dotted line with stars* is the IASP91 model and the *dotted line with small circles* is the PREM model

4. Resolution

Errors in our model may have several causes. One cause concerns the earthquake source parameters. The source mechanism would have little effect on our final models, but origin time, location and depth errors could change the velocities we found in our inversions. Another source of error could be the presence of lateral heterogeneity within the mantle sampled by the seismic waves that we invert. The inversion algorithm finds local minima solutions. Therefore, using different starting models results in different final models. By running inversions with several different starting models that result in similar fits to the data, we can estimate uncertainties and non-uniqueness in our final model. These issues are addressed in the next paragraphs. We used data from either the eastern or central models for our resolution testing since the data profiles from these models are similar in distance range and station density, and we assumed that the results from one profile hold for both profiles.

To determine whether source origin-time errors (and location/depth errors) map into the mantle structure, we change the origin time in steps of ± 1 , ± 3 , and ± 5 s for the eastern model (Fig. 7). The 3

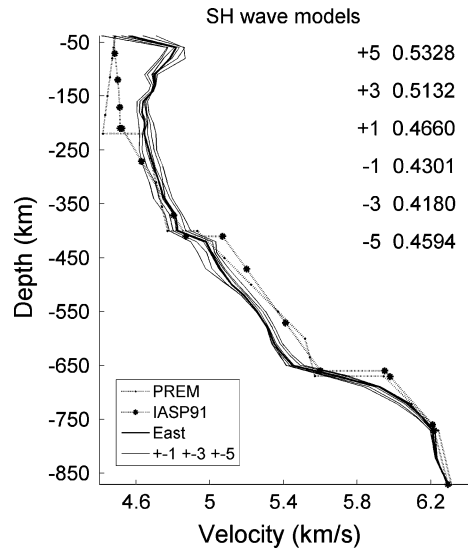


Figure 7

Eastern southern Africa SH velocity model (*heavy line*) plotted together with inverted models, where the source origin time has been changed in steps of ± 1 , ± 3 , and ± 5 s (*thin lines*). The *dotted line with stars* is the IASP91 model and the *dotted line with small circles* is the PREM model. The numbers refer to model misfits calculated with Eq. 2 for -5 to $+5$ s as described in the text

and 5 s changes in origin time shift the shallow-lid velocity within the models by up to 0.0468 and 0.0837 km/s, respectively, but do not change the gradients and sizes of the discontinuities appreciably. Misfits for $+1$ s to -1 s vary between 0.4660 and 0.4301, respectively, which is close to our best model misfit of 0.4692. The -3 s and -5 s shifts cause maximum changes between 150 and 180 km depth of -0.0186 and -0.0339 km/s, respectively. If the origin time is 5 s earlier, the resulting model is slower over most depths through the model, but the model still has a relatively small LVZ. We conclude that the origin-time errors result in a shifting of the entire model and do not affect gradients and discontinuity sizes appreciably, nor do they affect the general shape of the LVZ.

The eastern and central profiles map a region that could be affected by heterogeneity. This is because the earthquake is located in the East African Rift where slow shear velocities (3 to 4% slower than the global PREM model) extend to a depth of at least 250 km. The seismic stations, in turn, are located on the Kalahari craton, which has a near-vertical margin across which the shear velocity changes by as much

as 6% over a distance of 500 km (RITSEMA and VAN HEIJST, 2000). WANG *et al.* (2008) used a finite-difference method to test 2-D SH velocity structures along the path from the source that we are using to the Kalahari craton stations, accounting for different velocity structures outside and inside the craton. They found that the synthetics generated by the 2-D model did not improve synthetic fits over a 1-D model. Our results indicate that stations in the eastern profile with similar distances, which differ only in azimuth, show negligible relative time shifts (Figs. 1, 5a). Yet the data set shows a clear difference in waveforms for the central stations relative to the eastern stations (Fig. 3a). This implies that the region can be represented by two 1-D profiles, with negligible scattering caused by steep velocity changes across the craton boundary. We also determined above that the origin-time delays that might be caused by a slow lithospheric mantle at the earthquake source do not significantly change our results, except for a baseline shift in the model velocity.

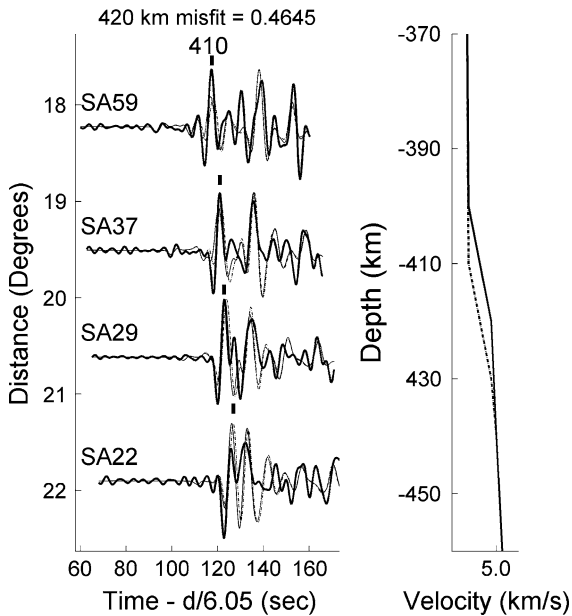


Figure 8

Four examples of central profile tangential component synthetics (*thin lines*) and data (*heavy lines*). The synthetic fits from Fig. 5b (*thin lines*) and the fits for a deeper discontinuity, 420 km deep (*dash-dot line*), are indicated, respectively for the corresponding models to the *right*. Arrivals labeled 410 are waves that reflect or turn near the 410 km discontinuity. The station names are listed on the *left*. The model misfit calculated with Eq. 2 is shown at the *top*

We apply forward modeling to estimate the uncertainty in depth and velocity jump of the 410 and 660 km discontinuities. For the 410 km discontinuity the depth and velocity jump obtained are 410 ± 10 km and ± 0.1 km/s, respectively, with the central model. The synthetic fits from Fig. 5b (*thin lines*) and the fits for a 420 km-deep discontinuity (*dash-dot line* in Fig. 8) are indicated for the corresponding model on the right in Fig. 8. The phase turning at 410 km depth is marked. The perturbed model misfit of 0.4645 indicates a worse fit than for our preferred model in Fig. 5b; the same holds for a 400 km discontinuity not shown in this paper. We applied a similar procedure to estimate the velocity jump uncertainty. However, for the 660 km discontinuity, only the two most distant stations recorded subtle arrivals from waves turning below the 660 km discontinuity, i.e., we have noisy data from only one station at large distances beyond 26° where the CD and EF branches extend. We determined a 660 ± 20 km discontinuity depth (but without velocity jump uncertainty) for the eastern region, even after we had given a higher weighting to the phases turning near 660 km depth to increase the sensitivity of the inversion. We assume that the velocity jump across the 660 km discontinuity is similar to that of the global models. The transition zone thickness is 250 ± 30 km. Discontinuity depths are best determined by vertical incidence-reflected waves, e.g., with receiver functions (GAO *et al.*, 2002; NIU *et al.*, 2004; BLUM and SHEN 2004), provided that the assumed velocity structure is accurate. Using turning waves better constrains velocity gradients, as well as the overall velocity jumps averaged over a discontinuity. However, small changes in the discontinuity depth do not change the averaged velocity jump, nor do they change the gradients above and below the discontinuity significantly.

An important issue regarding southern Africa's upper mantle structure is whether or not a significant LVZ exists. Both our eastern and central models have very moderate LVZs. The upper mantle shear models published by LI and BURKE (2006), PRIESTLEY (1999) and WANG *et al.* (2008) have strong LVZs (velocities less than 4.5 km/s near 200 to 300 km depth). In Fig. 9a we compare these models as well as the surface wave models without a significant LVZ by

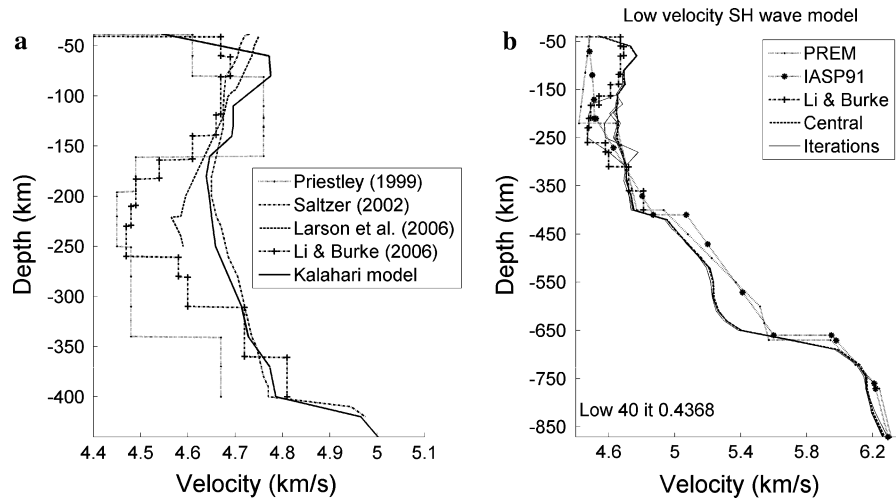


Figure 9

a Comparison of our preferred SH velocity Kalahari model (*solid line*) with four published shear velocity models for the Kalahari craton, two of which have strong low-velocity zones. The Kalahari model is an average of our eastern and central models for southern Africa. The models from PRIESTLEY (1999) (*dotted line with small circles*), LARSON *et al.* (2006) (*dashed line*) and LI and BURKE (2006) (*dash-dot line with pluses*) were derived from Rayleigh wave data, whereas SALTZER (2002) (*dash-dot line*) used both Rayleigh and Love waves. **b** Comparison of the central southern Africa SH velocity model (*heavy dashed line*) with the model from LI and BURKE (2006) (*dash-dot line with pluses*). The *thin lines* show the result of inversions for body waves for the low-velocity zone after 0, 16, 24, 32 and 40 iterations. The *dotted line with stars* is the IASP91 model and the *dotted line with small circles* is the PREM model. The model misfit calculated with Eq. 2 is shown at the *bottom left*

SALTZER (2002) and LARSON *et al.* (2006) with an average of our central and eastern models, which we will call the “Kalahari model”. We average the models for the shallow mantle study because they are very similar between 110 and 310 km depth. The models from PRIESTLEY (1999), LARSON *et al.* (2006) and LI and BURKE (2006) were derived from Rayleigh wave data, whereas SALTZER (2002) used both Rayleigh and Love waves.

To test whether our data allow for a strong LVZ, we use a starting model modified from that of LI and BURKE (2006) and then perform an inversion for the central profile with our selected origin time (Fig. 9b). We employ the same time window as in Fig. 5b and bandpass filter the first eight iterations between 0.01 and 0.07 Hz. This is followed by three more sets of eight iterations filtered with increasingly higher frequencies until the last set is filtered between 100 and 5 s (thin lines). Each intermediate result is the starting model for the next inversion after some smoothing. The misfit improves with each inversion to 0.4368 after 40 iterations, in comparison with the misfit of 0.4361 in Fig. 5b. With each new inversion

and improved misfit, the strong low-velocity zone is modified to a slight LVZ when compared with the central model (dashed line). We conclude that the data exclude a significant LVZ.

The primary data sets used in the surface-wave inversions were Rayleigh-wave phase velocities. It is likely that the difference between our SH velocity results and those of the mostly Rayleigh wave studies for the shallow mantle above 150 km (Fig. 9a) is due to the commonly observed phenomenon of anisotropy, such as is included in the PREM model (DZIEWONSKI and ANDERSON, 1981). The PREM model is anisotropic for the upper 200 km of the mantle, with an SH velocity faster than the SV, and where the SH velocity structure has a strong LVZ in comparison with the slight LVZ for SV. SH–SV wave anisotropy has been invoked to explain Love–Rayleigh wave discrepancies, although this is not strictly correct since Rayleigh wave velocity also depends on the anisotropic P-wave velocity structure.

More puzzling is the difference between our model and that published by WANG *et al.* (2008). WANG *et al.* used SH-wave data similar to our data

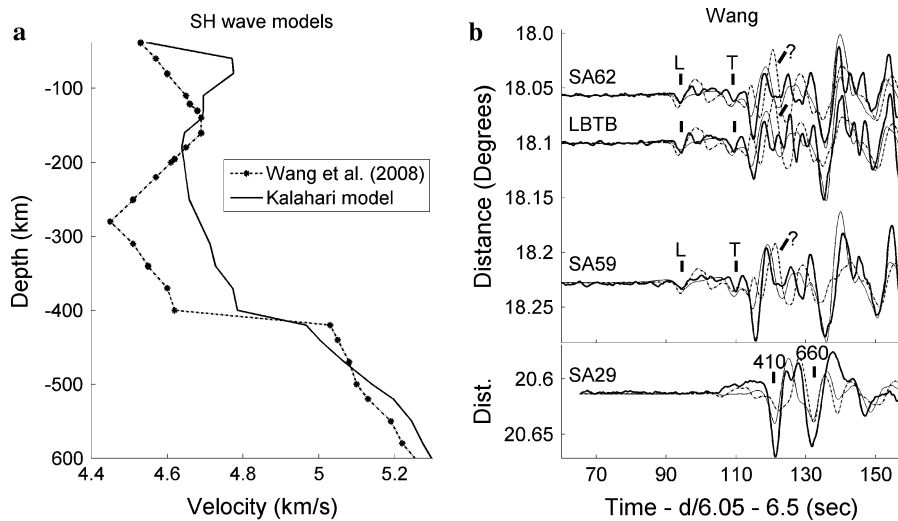


Figure 10

a Comparison of our preferred SH velocity Kalahari model (*solid line*) with the model of WANG *et al.* (2008) (*dash-dot line with stars*), who used SH body waves. **b** Four examples of synthetics computed using WANG *et al.*'s model (2008) (*dash-dot lines*) compared with the data (*heavy lines*) and synthetics computed using our central model (*thin lines*). The seismograms were integrated to simulate the displacement traces in Wang *et al.*'s publication. The station names are listed on the *left*. Arrivals labeled L travel through the high-velocity lid, arrivals labeled T are a tunneled, turning wave from below the lid, and arrivals labeled 410 and 660 are waves that reflect or turn near the 410 and 660 km discontinuities, respectively. An unmatched phase is labeled with a “?”

set, but concluded that there is a significant LVZ beneath the Kalahari craton (Fig. 10a). Part of the difference between our results and theirs is a difference in origin time but, as discussed above, a different origin time should result in a more uniform shift in velocity with depth and not create a large discrepancy in velocity from 200 to 350 km depth. In Fig. 10b we compare selected synthetics from our Kalahari model, as well as synthetics computed using Wang *et al.*'s model, with the data. In this comparison the data are displacement recordings, bandpass filtered from 0.05 to 1 Hz, as used in Wang *et al.*'s paper.

The two model synthetics are aligned on the first arrival to account for the different origin times (about 6.5 s). At these distance ranges both models produce a first arrival from the high-velocity lid (labeled L in Fig. 10b), a tunneled turning wave from below the lid (labeled T in Fig. 10b), lid multiples that are prominent at the short distances, and strong arrivals from the 410 and 660 km discontinuities. The Wang *et al.* model produces a large arrival from the 410 km discontinuity at a shorter distance than seen in the data ($\sim 18^\circ$), and also does not fit the timing of the

410 km arrival at longer distances (20° – 21°). The large out-of-phase misfits shown in Fig. 10b can also be seen in WANG *et al.*'s (2008) paper for all data from 17° to 19° . Although first arrival times can be fit equally well with both models using different origin times, we feel that the later arrivals, which are most sensitive to the velocities from 200 to 400 km depth, fit our model much better. The staged frequency inversion provides a more robust inversion approach than trial-and-error modeling.

Another important issue is whether the mantle transition zone under southern Africa differs from the global PREM (DZIEWONSKI and ANDERSON, 1981) and IASP91 models (KENNETT and ENGDahl, 1991). Both our eastern and central models have less-steep velocity gradients (Fig. 6), with central velocities of less than 5.4 km/s above the 660 km discontinuity. To test whether our data allow for a steeper velocity gradient, we use as a starting model for the transition zone the global PREM model (DZIEWONSKI and ANDERSON, 1981) (Fig. 11a). The synthetic fits from Fig. 5a (thin lines) and the fits for a steeper velocity gradient (dash-dot lines in Fig. 11a) are indicated for the corresponding model on the right. Note that we

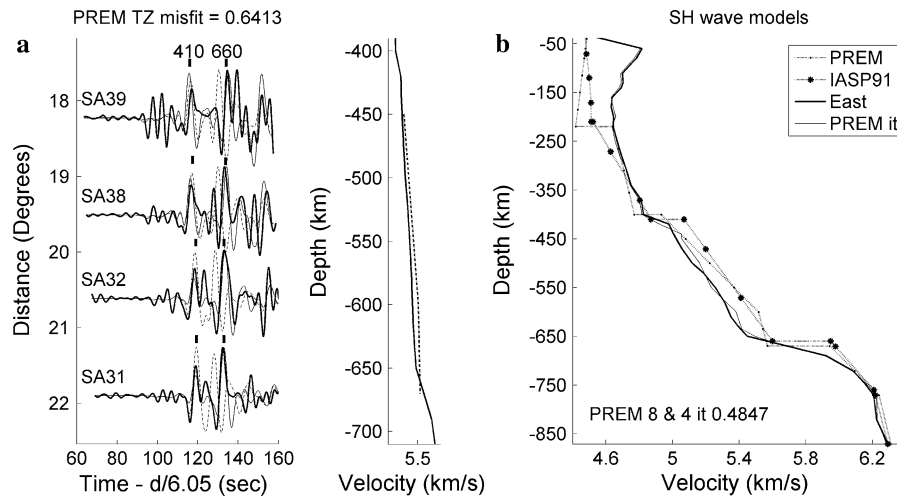


Figure 11

a Four examples of eastern profile tangential component synthetics and data (*heavy lines*). The synthetic fits from Fig. 5a (*thin lines*) and the fits for the mantle transition zone with a steeper velocity gradient from the global PREM model (*dash-dot line*) are indicated, respectively, for the corresponding models to the *right*. The station names are listed on the *left*. The model misfit calculated with Eq. 2 is shown at the *top*. **b**. Comparison of the eastern southern Africa SH velocity model (*heavy line*) with the IASP91 model (*dotted line with stars*) and PREM model (*dotted line with small circles*). The *thin line* shows the result of an inversion consisting of 12 iterations using the model in Fig. 11a as the starting model

had already established that the depths of the transition zone boundaries are 410 ± 10 km and 660 ± 20 km. Phase arrivals turning at the 410 and 660 km discontinuities are marked and this start model has a misfit of 0.6413. The PREM model converged to a final misfit of 0.4847 shown in Fig. 11b. This was after eight iterations with a bandpass filter between 0.01 and 0.08 Hz, followed by four more iterations filtered between 100 and 5 s. The result in Fig. 11b has the same, less-steep velocity gradient as in Fig. 6. The lower gradient and slower velocities in the transition zone relative to the PREM model are well constrained.

5. Discussion

5.1. Lithospheric and Shallow Structure above 410 km

The two models derived in this study sample mantle beneath several tectonic units within the Kalahari craton in southern Africa. The Kalahari craton is comprised of the Archean Kaapvaal and Zimbabwe cratons connected by the Limpopo belt and surrounded by Paleo- and Mesoproterozoic orogenic belts (Fig. 1). The cratonic core has been

a stable assemblage for the past 2.0 Ga. The velocity models are similar, except above 110 km depth where the eastern profile is slightly faster, and above the 410 km discontinuity where the central profile is slower, resulting in a larger velocity jump across it (Fig. 6). Surface-wave studies of southern Africa also show a similar east-to-west gradient in the shallow mantle velocity (PRIESTLEY *et al.*, 2006). It is unlikely that the lid difference is due to temperature variations since the lid is confined to very shallow depths. We interpret this difference as due either to fossil anisotropy within the lithosphere or to a compositional gradient between the profiles at very shallow depth. Their observations of shear-wave splitting and surface waves led SILVER *et al.* (2004) to conclude that the eastern Kaapvaal shield is almost isotropic. There is a spatially continuous arc of anisotropic mantle extending from the western and northwestern Kaapvaal craton to the Limpopo and Magondi belts and hence to the Zimbabwe craton. The isotropic–anisotropic transition (from our eastern and central profiles) is relatively sharp and correlates with the difference in waveforms we observe for the two profiles.

The central model partially samples the Proterozoic Kheis belt which developed at the western

margin of the Kaapvaal craton c. 1.75 Ga (Fig. 1). It is comprised of a fold-and-thrust belt and consists of dipping arenitic metasediments, as well as explosive volcanic and intrusive rocks, as opposed to the geologically simpler Archean Kaapvaal craton (MOEN, 1999). GRIFFIN *et al.* (2003) note a difference in xenolith depletion between the Kheis belt and the central Archean areas of the Kalahari craton. Our overall results show differences in lid velocity between Archean (older than 2,600 Ma) terrains and Proterozoic terrains to depths up to 110 km, and also show slower velocity for central southern Africa above the 410 km discontinuity (Fig. 6).

Our lithospheric and shallow mantle shear velocity models above 410 km for the Kalahari craton (the average of the eastern and western models) are similar to the SH model by SALTZER (2002) in that there are high SH-wave speeds in the lithosphere, with a slight LVZ beneath reaching minimum velocities between 160 and 200 km depth (Fig. 9a). In our model the decrease in velocity begins near 110 km depth, similar to the depth at which HANSEN *et al.* (2009) find a decrease in shear velocity using S-wave receiver functions. We found no evidence for a significant LVZ beneath the Kalahari craton of southern Africa as presented by PRIESTLEY (1999), LI and BURKE (2006) and WANG *et al.* (2008). The surface-wave models are slower for the shallow lid than our Kalahari model, but they were derived using Rayleigh waves and, as discussed in FREYBOURGER *et al.* (2001) and SALTZER (2002), there is weak-to-moderate anisotropy beneath the Kalahari, with Love waves indicating faster velocities than Rayleigh waves. This may be a cause of the discrepancy between our model and the models derived from Rayleigh waves.

In Fig. 12 we compare our Kalahari craton SH velocity model with SH velocity models derived from data sampling the Canadian Shield (GRAND and HELMBERGER, 1984) and the east European platform (MATZEL and GRAND, 2004). As all the models were derived from the same type of data, i.e., 10–20 s period regional SH-waves, they should be directly comparable. The most striking difference in the lithospheric mantle between the Kalahari model and the other craton models is the thinner lid beneath southern Africa, although all these craton models are

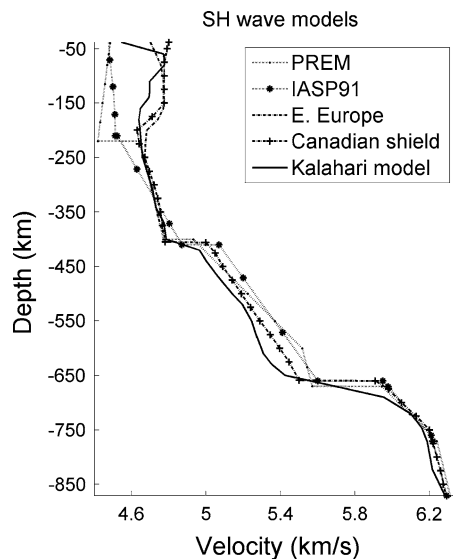


Figure 12
Comparison of our preferred SH velocity Kalahari model (*heavy line*) with the IASP91 model (*dotted line with stars*) and PREM model (*dotted line with small circles*). The Kalahari model is an average of our eastern and central models for southern Africa. It is also compared with the east European platform model of MATZEL AND GRAND (2004) (*dash-dot line*) and model SNA (*dash-dot line with pluses*) which was derived from data sampling the Canadian Shield (GRAND and HELMBERGER, 1984)

much faster than PREM or IASP91 in the upper 200 km. The lid is identified under the Kalahari by a negative velocity gradient beginning at 110 km, whereas the LVZs of the Canadian Shield and the east European platform begin at 180 and 190 km, respectively. Underneath the lid there is a reduced negative velocity gradient in contrast to the Canadian Shield and the east European platform. The shear velocity below 200 km is similar to that beneath the Kalahari and the other cratons. The recent surface-wave tomography model of PRIESTLEY *et al.* (2008) also shows the deep lithosphere of the Kalahari craton to be seismically slightly slower than that of the other African cratons. The difference in negative velocity gradient at the base of the lithosphere is predicted by the conceptual model of NYBLADE and SLEEP (2003), in which a plume with a narrow tail has spread beneath the lithosphere below the Kalahari craton, thus heating the lower lithosphere over a wide area but not broadly heating the deeper mantle.

The compositional structure and thermal state of the lithospheric mantle beneath the Kalahari craton and

the surrounding mobile belts have been extensively mapped before, using garnet xenocrysts from kimberlites (e.g., GRIFFIN *et al.*, 2003; WILSON *et al.*, 2007) (Fig. 1). GRIFFIN *et al.* (2003) conclude that each terrain may have carried its own lithospheric keel from the time of craton amalgamation, 2.6–2.7 Ga. The lithospheric mantle beneath the Proterozoic crust of the Kheis belt (sampled by our central region, Fig. 1) is less depleted, i.e., more iron-rich with $Mg\# = 100 \times Mg/(Mg + Fe) > \sim 91.5$, than that beneath the central Archean areas of the Kalahari craton. From inter-element correlations using multivariate statistics, GRIFFIN *et al.* (2003) recognized 14 distinctive populations for xenoliths from kimberlites in southern Africa. They grouped these into four major categories: depleted $93.6 < Mg\# < 91.6$; depleted/metasomatized $93.2 < Mg\# < 92.0$; fertile lherzolite $92.1 < Mg\# < 87.4$; and melt-metasomatized $91.7 < Mg\# < 90.3$. An analysis of the xenoliths in terms of elements and the major groups suggests that, due to sublithospheric melt intrusion into the base (as also proposed by NYBLADE and SLEEP, 2003), metasomatism refertilized the base between 117 and 108 Ma (GRIFFIN *et al.*, 2003; KOBUSSEN *et al.*, 2008). This is identifiable or pronounced for all the kimberlite xenoliths analyzed, except for the Namaqua belt. Refertilization would increase the mean density, whereas the corresponding rise in the geotherm would decrease the mean density. We propose that the difference in deep lithosphere shear velocity between the Kalahari craton and the other two cratons is due to both heating and, to a lesser extent, refertilization during the Mesozoic, as suggested by GRIFFIN *et al.* (2003) and KOBUSSEN *et al.* (2008).

It is not possible to determine from shear velocity alone the relative importance of the compositional and temperature anomalies that explain the difference between the Canadian, east European and Kalahari cratonic lithospheric mantle. Figure 13 (graph a) shows the difference in shear velocity between our Kalahari model and the model derived for the east European platform as a function of depth. Graphs b and c in Fig. 13 show the differences in Mg# and temperature, respectively, which explain the differences in seismic velocity between east Europe and the Kalahari. Also shown are the implied density differences explaining the compositional and

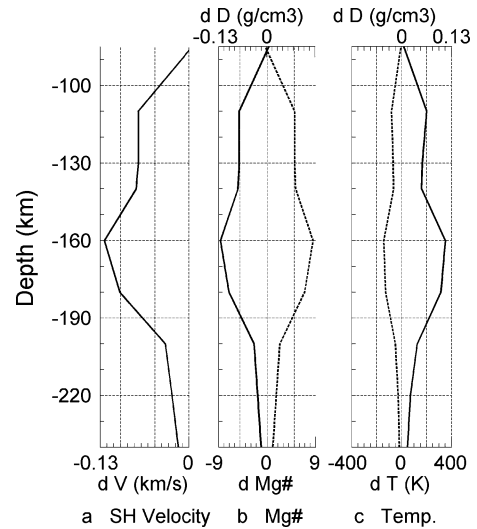


Figure 13

The velocity difference between the Kalahari model and the eastern European platform (a). Panel b shows the change in Mg# (solid line) required to explain the velocity difference between the two models shown in Fig. 12, as well as the corresponding difference in density (dashed line) using the results from LEE (2003). Panel c shows the temperature difference (solid line) needed to explain the velocity difference, using results from CAMMARANO *et al.* (2003) with the corresponding density difference (dashed line) using results from LEE (2003)

temperature anomalies. Mg# is likely to be a good proxy for summarizing the chemical changes due to metasomatic refertilization.

We apply the shear velocity to Mg# and density to Mg# scalings given by LEE (2003) for spinel and garnet-peridotite samples at standard temperature and pressure (STP). The scaling of temperature to shear velocity is taken from CAMMARANO *et al.* (2003) for a dry pyrolytic mantle, and a thermal expansion coefficient from LEE (2003) is used to estimate the corresponding density anomaly. It should be noted that SCHUTT and LESHER (2006) find that melt depletion of fertile lherzolite has little effect on shear velocity, so that larger Mg# changes would be required in Fig. 13 (graph b) to explain the observed seismic differences. A purely compositional interpretation of the velocity difference yields a maximum Mg# change of ~ -8.7 , but an average over a 110 km depth range (from 110 to 220 km) of ~ -4.3 . The Mg# difference between GRIFFIN *et al.*'s (2003) fertile lherzolite and depleted/metasomatized classes is ~ -2.9 . A purely thermal interpretation of the

velocity anomaly would require a peak temperature increase of ~ 350 K, with an average over 110 km of ~ 170 K. In comparison, NYBLADE and SLEEP'S (2003) model yielded mantle material with an excess temperature of ~ 200 K impinging on the lithosphere 183 m.y. ago, with more episodes 90–80 m.y. ago associated with kimberlite eruptions that caused heat to diffuse slowly throughout the whole lithosphere. Their model predicts that today the lithosphere has cooled to an excess temperature of ~ 90 K at 100 km depth, with ~ 25 km of lithospheric thinning.

The Kalahari craton has an elevation roughly 1 km higher than the Canadian and European cratons, which is appropriate to the velocity models shown in Fig. 12. The Kalahari and east Europe crustal structures do not differ significantly. The east European platform has a slightly thicker crust of ~ 42 km (NIU and JAMES, 2002; MOONEY *et al.*, 1998) compared with 35–40 km for the Kalahari. Thus, the high elevation of the Kalahari relative to east Europe is not due to differences in the crust. If the high elevation of the Kalahari relative to the other shields were due to buoyancy of the lower 110 km of lithosphere, an average density difference of ~ 0.05 g/cm³ over that depth extent would be required. The average temperature anomaly of 170 K over 110 km thickness needed to explain the difference in shear velocities between the cratons (Fig. 13) would decrease the density by ~ -0.023 g/cm³, using the thermal expansion coefficient given by LEE (2003). Thus, even if the difference in shear velocity we observe between the Kalahari craton and the Canadian and east European cratons were due entirely to relatively high temperatures in the deep lithosphere, this would account for less than half of the anomalously high elevation of southern Africa. If we assume an excess temperature of 90 K over a 110 km depth range, as predicted by NYBLADE and SLEEP'S (2003) model, and a corresponding difference in Mg# of ~ -2 between the Kalahari and the other cratons, this would match the seismic difference but would result in essentially no buoyancy difference or a slightly negative one of ~ -0.017 g/cm³ in the deep lithosphere.

We conclude that the high elevation of the Kalahari craton cannot be explained by shallow mantle (upper 400 km) buoyancy alone. A maximum of $\sim 50\%$ of the elevation could come from lower

lithosphere buoyancy if all seismic variation is due to temperature but, given the results of KOBUSSEN *et al.* (2008), it is likely the Mg# beneath the Kalahari is less than beneath the east European platform and this would lessen the buoyancy further. Thus, deep mantle processes are likely to be the cause of the high Kalahari elevation, and consequently for much of the anomalous elevation of the African superswell, at least across southern Africa.

5.2. Deep Structure

The deeper parts of our two models are similar to those of global models with discontinuity depths near 410 ± 10 and 660 ± 20 km. The transition zone thickness of 250 ± 30 km is close to the global average of 242 km (LAWRENCE and SHEARER, 2006a). The difference is probably within the error bars of our turning wave study and agrees with the more accurate, vertical-incidence receiver-function result of, e.g., NIU *et al.* (2004). However, the velocity structure of the transition zone in our models is quite different from that of the global average models PREM and IASP91 (Figs. 6, 12). The eastern model has a smaller velocity jump than PREM at 410 km, whereas the central model's jump is larger. Both models are slower overall, with a correspondingly less steep velocity gradient between the discontinuities, and the central model is much slower from near 500 to 650 km depth. This could indicate a thermal or chemical anomaly in this depth range with respect to the PREM and IASP91 models, and compositional changes from east to west beneath southern Africa, although the 410 and 660 km discontinuity depths argue against strong temperature anomalies. On the other hand, the global models may not be accurate in detail within the transition zone. Other regional models with a slower transition zone velocity structure or a less-steep gradient have also been derived for North America (e.g., model SNA for the Canadian shield, GRAND and HELMBERGER (1984), see Fig. 12) and beneath eastern Mexico, as recorded by the La Ristra array (GAO *et al.*, 2006). In a global study LAWRENCE and SHEARER (2006b) found an average jump of 7.0% in shear velocity at 410 km depth, which is larger than that found in the central model and much larger than that in the PREM model. We

conclude that the deep transition zone shear velocity may be anomalously slow beneath southern Africa, with compositional changes from east to west, but there is still too much uncertainty in global reference models to quantify the anomaly. It should also be noted that no global tomography model shows a slow seismic anomaly near 600 km depth beneath southern Africa. This highlights the need to further refine global velocity models to improve interpretations of mantle transition zone temperature and compositional variations.

6. Conclusion

We have developed upper mantle shear velocity models along two profiles through southern Africa. Both models show high-velocity lithospheric mantle lids, but there is an east-to-west gradient in shear velocity in the upper 110 km. The shear velocity beneath the Kalahari craton is similar to the shear velocities found beneath other cratons, with slightly slower velocities in the deep lithosphere. These slower velocities may be due to a combination of higher temperatures and, to a lesser extent, chemical changes due to metasomatism and/or melt infiltration. We find that less than half of the anomalously high elevation of the Kalahari craton can result from the deep lithosphere if the seismic anomaly is purely thermal. For a model with an excess temperature of ~ 90 K over a 110 km thickness, together with a Mg# change of ~ 2 caused by metasomatism and/or melt infiltration, there is essentially no anomalous buoyancy associated with the lithosphere, but there is a change in shear velocity which matches our observations.

Velocity jumps across the 410 and 660 km discontinuities differ between the eastern and central profiles, and both are different from those in the PREM model. We obtained less-steep shear velocity gradients, especially for central southern Africa, below 500 km depth relative to the PREM and IASP91 models, although the transition zone thickness is close to the global average. The slow seismic structure just above 600 km depth may indicate a thermal or chemical anomaly and/or compositional changes from east to west at that depth. However, it is

more likely to be an indication that the global models are not accurate in detail in the transition zone. Our seismic results show little support for an upper mantle source of buoyancy for the unusually high elevation of the Kalahari craton, and hence the portion of the African superswell in southern Africa. Rather, our results support a deep mantle cause for the high elevation, as proposed by LITHGOW-BERTELLONI and SILVER (1998) and GURNIS *et al.* (2000).

Acknowledgments

The authors wish to thank Eric Matzel for many discussions about conjugate gradient waveform inversion methodology and for use of his code, and an anonymous reviewer for helpful comments. We would also like to thank Bill Griffin for providing information on xenoliths recovered from the Kalahari craton. We thank the University of the Witwatersrand, South Africa, for providing administrative support and the Council for Geoscience, South Africa, for granting the corresponding author study leave to spend time at the University of Texas at Austin. This research was supported by NSF grants EAR-0440222, EAR-0440032, and OISE 0530062. Language editing and styling was done by Beverlie Davies.

REFERENCES

- BINA, C.R. and HELFFRICH, G. (1994), *Phase transition Clapeyron slopes and transition zone seismic discontinuity tomography*, Journal of Geophysical Research, 99, 15,853–15,860.
- BLOCH, S., HALES, A.L. and LANDISMAN, M. (1969), *Velocities in the crust and upper mantle of Southern Africa from multi-mode surface wave dispersion*, Bulletin of the Seismological Society of America, 59, 1599–1629.
- BLUM, J. and SHEN, Y. (2004), *Thermal, hydrous, and mechanical states of the mantle transition zone beneath Southern Africa*, Earth and Planetary Science Letters, 217, 367–378.
- CAMMARANO, F., GOES, S., VACHER, P. and GIARDINI, D. (2003), *Inferring upper-mantle temperatures from seismic velocities*, Physics of the Earth and Planetary Interiors, 138, 197–222.
- CARLSON, R., GROVE, T., DE WIT, M. and GURNEY, J. (1996), *Anatomy of an Archean craton: A program for interdisciplinary studies of the Kaapvaal craton, southern Africa*, EOS Transactions AGU, 77, 273–277.
- DZIEWONSKI, A.M. and ANDERSON, D.L. (1981), *Preliminary reference Earth model*, Physics of the Earth and Planetary Interiors, 25, 297–356.

- DZIEWONSKI, A.M. (1984), *Mapping the lower mantle: Determination of lateral heterogeneity in P velocity up to degree and order 6*, Journal of Geophysical Research, 89, 5929–5952.
- FOUCH, M.J., JAMES, D.E., VANDECAR, J.C. VAN DER LEE, S. and the KAAPVAAL SEISMIC GROUP (2004), *Mantle seismic structure beneath the Kaapvaal and Zimbabwe cratons*, South African Journal of Geology, 107, 33–44.
- FREYBOURGER, M., GAHERTY, J.B., JORDAN, T.H. and the KAAPVAAL SEISMIC GROUP (2001), *Structure of the Kaapvaal craton from surface waves*, Geophysical Research Letters, 28, 2489–2492.
- FUCHS, K. and MÜLLER, G. (1971), *Computation of synthetic seismograms with the reflectivity method and comparison with observations*, Geophysical Journal of the Royal Astronomical Society, 23, 417–433.
- GAO, S.S., SILVER, P.G. and LIU, K.H. (2002), *Mantle discontinuities beneath Southern Africa*, Geophysical Research Letters, 29, 1291–1294.
- GAO, W., MATZEL, E. and GRAND, S.P. (2006), *Upper mantle seismic structure beneath eastern Mexico determined from P and S waveform inversion and its implications*, Journal of Geophysical Research, 111, B08307, doi:10.1029/2006JB004304.
- GRAND, S.P. (2002), *Mantle shear-wave tomography and the fate of subducted plates*, Philosophical Transactions of the Royal Society of London, 360, 2475–2491.
- GRAND, S.P. and HELMBERGER, D.V. (1984), *Upper mantle shear structure of North America*, Geophysical Journal of the Royal Astronomical Society, 76, 399–438.
- GRIFFIN, W.L., O'REILLY, S.Y., NATAPOV, L.M. and RYAN, C.G. (2003), *The evolution of lithospheric mantle beneath the Kalahari Craton and its margins*, Lithos, 71, 215–241, doi:10.1016/j.lithos.2003.07.006.
- GU, Y.J., DZIEWONSKI, A.M., SU, W. and EKSTROM, G. (2001), *Models of the mantle shear velocity and discontinuities in the pattern of lateral heterogeneity*, Journal of Geophysical Research, 106, 11,169–11,199.
- GURNIS, M., MITROVICA, J.X., RITSEMA, J.E. and VAN HEIJST, H.-J. (2000), *Constraining mantle density structure using geological evidence of surface uplift rates: The case of the African Superplume*, Geochemistry Geophysics Geosystems, 1(7), doi:10.1029/1999GC000035.
- HAGER, B.H., CLAYTON, R.W., RICHARDS, M.A., COMER, R.P. and DZIEWONSKI, A.M. (1985), *Lower mantle heterogeneity, dynamic topography and the geoid*, Nature, 313, 541–545.
- HANSEN, S.E., NYBLADE, A.A., JULIA, J., DIRKS, P.H.G.M. and DURRHEIM, R.J. (2009), *Upper mantle Low-Velocity Zone structure beneath the Kaapvaal craton from S-wave receiver functions*, Geophysical Journal International (accepted for publication).
- KENNETT, B.L.N. and ENGDALH, E.R. (1991), *Traveltimes for global earthquake location and phase identification*, Geophysical Journal International, 105, 429–465.
- KOBUSSEN, A.F., GRIFFIN, W.L.S., O'REILLY, Y. AND SHEE, S.R. (2008), *Ghosts of lithospheres past: Imaging an evolving lithospheric mantle in Southern Africa*, Geology, 36, 515–518, doi:10.1130/G24868A.1.
- LARSON, A. M., SNOKE, A. and JAMES, D.E. (2006), *S-wave velocity structure, mantle xenoliths, and the upper mantle beneath the Kaapvaal craton*, Geophysical Journal International, 167, 171–186, doi:10.1111/j.1365-246X.2006.03005.x.
- LAWRENCE, J.F. and SHEARER, P.M. (2006a), *A global study of transition zone thickness using receiver functions*, Journal of Geophysical Research, 111, doi:10.1029/2005JB003973.
- LAWRENCE, J. F. and SHEARER, P.M. (2006b), *Constraining seismic velocity and density for the mantle transition zone with reflected and transmitted waveforms*, Geochemistry Geophysics Geosystems, 7, doi:10.1029/2006GC001339.
- LEE, C.-T.A. (2003), *Compositional variation of density and seismic velocities in natural peridotites at STP conditions: Implications for seismic imaging of compositional heterogeneities in the upper mantle*, Journal of Geophysical Research, 108(B9), 2441, doi:10.1029/2003JB002413.
- LI, A. and BURKE, K. (2006), *Upper mantle structure of Southern Africa from Rayleigh wave tomography*, Journal of Geophysical Research, 111, B10303, doi:10.1029/2006JB004321.
- LITHGOW-BERTELLONI, C. and SILVER, P.G. (1998), *Dynamic topography, plate driving forces and the African superswell*, Nature, 395, 269–272.
- MASTERS, T.G., LASKE, G., BOLTON, H. and DZIEWONSKI, A. (2000), *The relative behaviour of shear velocity, bulk sound speed and compressional velocity in the mantle: Implications for chemical thermal structure, in Earth's deep interior. Mineral physics and tomography from the atomic to the global scale.* (S. KARATO et al., eds), AGU Geophysical Monograph, 117, 63–87. Washington, DC, USA.
- MATZEL, E. (2002), *The anisotropic seismic structure of the Earth's mantle: Investigations using full waveform inversion*, PhD dissertation, The University of Texas at Austin, USA.
- MATZEL, E. and GRAND, S.P. (2004), *The anisotropic seismic structure of the East European platform*, Journal of Geophysical Research, 109, B01302, doi:10.1029/2001JB000623.
- MEGNIN, C. and ROMANOWICZ, B. (2000), *The three-dimensional shear velocity structure of the mantle from the inversion of body, surface and higher-mode waveforms*, Geophysical Journal International, 243, 709–728.
- MELBOURNE, T. and HELMBERGER, D.V. (1998), *Fine structure of the 410 km discontinuity*, Journal of Geophysical Research, 103, 10,091–10,102.
- MOEN, H.F.G. (1999), *The Kheis Tectonic Subprovince, Southern Africa: A lithostratigraphic perspective*, South African Journal of Geology, 102(1), 27–42.
- MOONEY, W.D., LASKE, G. and MASTERS, T.G. (1998), *CRUST 5.1: A global crustal model at 5° × 5°*, Journal of Geophysical Research, 103, 727–747.
- MORA, P. (1988), *Elastic wave-field inversion of reflection and transmission data*, Geophysics, 53(6), 750–759.
- NGUURI, T.K., GORE, J., JAMES, D.E., WEBB, S.J., WRIGHT, C., ZENGENI, T.G., GWAVAVA, O., SNOKE, J.A. and KAAPVAAL SEISMIC GROUP (2001), *Crustal structure beneath Southern Africa and its implication for the formation and evolution of the Kaapvaal and Zimbabwe cratons*, Geophysical Research Letters, 28, 2501–2504.
- NI, S., TAN, E., GURNIS, M. and HELMBERGER, D. (2002), *Sharp sides to the African Superplume*, Science, 296, 1850–1852.
- NI, S., HELMBERGER, D.V. and TROMP, J. (2005), *Three-dimensional structure of the African superplume from waveform modeling*, Geophysical Journal International, 161, 283–294.
- NIU, F. and JAMES, D.E. (2002), *Fine structure of the lowermost crust beneath Kaapvaal craton and its implications for crustal formation and evolution*, Earth and Planetary Science Letters, 200, pp. 121–130.
- NIU, F., LEVANDER, A., COOPER, C. M., LEE, C.A., LENARDIC, A. and JAMES, D.E. (2004), *Seismic constraints on the depth and*

- composition of the mantle keel beneath the Kaapvaal craton*, Earth and Planetary Science Letters, 224, 337–346.
- NYBLADE, A. and LANGSTON, C.A. (1998), *Upper mantle P wave velocities beneath Southern Africa and the origin of the African Superswell*, Southern African Geophysical Review, 2, 55–61.
- NYBLADE, A. and ROBINSON, S. (1994), *The African Superswell*, Geophysical Research Letters, 21, 765–768.
- NYBLADE, A.A. and SLEEP, N.H. (2003), *Long-lasting epeirogenic uplift from mantle plumes and the origin of the Southern African Plateau*, Geochemistry Geophysics Geosystems, 4(12), doi: [10.1029/2003GC000573](https://doi.org/10.1029/2003GC000573).
- PRIESTLEY, K. (1999), *Velocity structure of the continental upper mantle: Evidence from Southern Africa*, Lithos, 48, 45–56.
- PRIESTLEY, K., MCKENZIE, D. and DEBAYLE, E. (2006), *The state of the upper mantle beneath Southern Africa*, Tectonophysics, 416, 101–112.
- PRIESTLEY, K., MCKENZIE, D., DEBAYLE, E. and PILIDOU, S. (2008), *The African upper mantle and its relationship to tectonics and surface geology*, Geophysical Journal International, 175, 1108–1126.
- QIU, X., PRIESTLY, K. and MCKENZIE, D. (1996), *Average lithospheric structure of Southern Africa*, Geophysical Journal International, 127, 563–587.
- RITSEMA, J., NI, S., HELMBERGER, D. V. and CROTWELL, H. P. (1998), *Evidence for strong shear velocity gradients in the lower mantle beneath Africa*, Geophysical Research Letters, 25, 4245–4248.
- RITSEMA, J., VAN HEIJST, H. J. and WOODHOUSE, J. H. (1999), *Complex shear wave velocity structure imaged beneath Africa and Iceland*, Science, 286, 1925–1928.
- RITSEMA, J. and VAN HEIJST, H.J. (2000), *New seismic model of the upper mantle beneath Africa*, Geology, 28, 63–66.
- SALTZER, R. (2002), *Upper mantle structure of the Kaapvaal craton from surface wave analysis—a second look*, Geophysical Research Letters, 29(6), doi: [10.1029/2001GL013702](https://doi.org/10.1029/2001GL013702).
- SCHUTT, D.L. and LESHER, C.E. (2006), *Effects of melt depletion on the density and seismic velocity of garnet and spinel lherzolite*, Journal of Geophysical Research, 111, B05401, doi: [10.1029/2003JB002950](https://doi.org/10.1029/2003JB002950).
- SILVER, P.G., FOUCH, M.J., GAO, S.S. and SCHMITZ, M. (2004), *Seismic anisotropy, mantle fabric, and magmatic evolution of Precambrian Southern Africa*, South African Journal of Geology, 107, 45–58.
- SIMMONS, N.A., FORTE, A.M. and GRAND, S.P. (2007), *Thermochemical structure and dynamics of the African superplume*, Geophysical Research Letters, 34, L02301, doi: [10.1029/2006GL028009](https://doi.org/10.1029/2006GL028009).
- SIMON, R.E., WRIGHT, C.E., KGASWANE, M. and KWADIBA, M.T.O. (2002), *The P wavespeed structure below and around the Kaapvaal craton to depths of 800 km, from traveltimes and waveforms of local and regional earthquakes and mining-induced tremors*, Geophysical Journal International, 151, 132–145.
- SIMON, R.E., WRIGHT, C., KWADIBA, M.T.O. and KGASWANE, E.M. (2003), *Mantle structure and composition to 800-km depth beneath Southern Africa and surrounding oceans from broadband body waves*, Lithos, 71, 353–367.
- STANKIEWICZ, J., CHEVROT, S., VAN DER HILST, R.D. and DE WIT, M.J. (2002), *Crustal thickness, discontinuity, and upper mantle structure beneath Southern Africa: constraints from body wave inversions*, Physics of the Earth and Planetary Interiors, 130, 235–251.
- TANKARD, A. J., JACKSON, M.P.A., ERIKSSON, K.A., HOBDAJ, D.K., HUNTER, D.R. and MINTER, W.E.L. (1982), *Crustal Evolution of Southern Africa* (Springer-Verlag New York 1982).
- VINNIK, L.P., GREEN, R.W.E., NICOLAYSEN, L.O., KOSAREV, G.L. and PETERSEN, N.V. (1996), *Deep seismic structure of the Kaapvaal craton*, Tectonophysics, 262, 67–75.
- WANG, Y., WEN, L. and WEIDNER, D. (2008), *Upper mantle SH- and P-velocity structures and compositional models beneath Southern Africa*, Earth and Planetary Science Letters, 267, 596–608.
- WILSON, M.G.C., MCKENNA, N. and LYNN, M.D. (eds) (2007), *The occurrence of diamonds in South Africa*, Mineral Resources Series No. 1, Council for Geoscience and De Beers, Pretoria, South Africa.
- WRIGHT, C., KWADIBA, M.T.O., KGASWANE, E.M. and SIMON, R.E. (2002), *The structure of the crust and upper mantle to depths of 320 km beneath the Kaapvaal craton, from P wave arrivals generated by regional earthquakes and mining-induced tremors*, Journal of African Earth Sciences, 35, 477–488.
- ZHAO, M., LANGSTON, C. A. and NYBLADE, A.A. (1999), *Upper mantle velocity structure beneath Southern Africa from modelling regional seismic data*, Journal of Geophysical Research, 104, 4783–4794.

(Received January 5, 2011, revised May 9, 2011, accepted May 31, 2011)